



# ElaStic: A tool for calculating second-order elastic constants from first principles



Rostam Golesorkhtabar<sup>a,b,\*</sup>, Pasquale Pavone<sup>a,b,1</sup>, Jürgen Spitaler<sup>a,b</sup>, Peter Puschnig<sup>a,2</sup>, Claudia Draxl<sup>a,1</sup>

<sup>a</sup> Chair of Atomistic Modelling and Design of Materials, Montanuniversität Leoben, Franz-Josef-Straße 18, A-8700 Leoben, Austria

<sup>b</sup> Materials Center Leoben Forschung GmbH, Roseggerstraße 12, A-8700 Leoben, Austria

## ARTICLE INFO

### Article history:

Received 19 June 2012

Received in revised form

27 February 2013

Accepted 12 March 2013

Available online 21 March 2013

### Keywords:

Elasticity

Second-order elastic constants

First-principles calculations

Density-functional theory

## ABSTRACT

Elastic properties play a key role in materials science and technology. The elastic tensors at any order are defined by the Taylor expansion of the elastic energy or stress in terms of the applied strain. In this paper, we present ElaStic, a tool that is able to calculate the full second-order elastic stiffness tensor for any crystal structure from *ab initio* total-energy and/or stress calculations. This tool also provides the elastic compliances tensor and applies the Voigt and Reuss averaging procedure in order to obtain an evaluation of the bulk, shear, and Young moduli as well as the Poisson ratio of poly-crystalline samples. In a first step, the space-group is determined. Then, a set of deformation matrices is selected, and the corresponding structure files are produced. In a next step, total-energy or stress calculations for each deformed structure are performed by a chosen density-functional theory code. The computed energies/stresses are fitted as polynomial functions of the applied strain in order to get derivatives at zero strain. The knowledge of these derivatives allows for the determination of all independent components of the elastic tensor. In this context, the accuracy of the elastic constants critically depends on the polynomial fit. Therefore, we carefully study how the order of the polynomial fit and the deformation range influence the numerical derivatives, and we propose a new approach to obtain the most reliable results. We have applied ElaStic to representative materials for each crystal system, using total energies and stresses calculated with the full-potential all-electron codes *exciting* and WIEN2k as well as the pseudo-potential code Quantum ESPRESSO.

© 2013 Elsevier B.V. All rights reserved.

## 1. Introduction

The investigation of second-order elastic constants (SOECs) is an essential research topic in materials science and technology as they govern the mechanical properties of a material. Thus, much effort is put on their calculation and measurement. Moreover, SOECs are related to inter-atomic potentials, phonon spectra, structural stability and phase transitions, as well as the equation of state. They also enter thermodynamical properties like specific heat, thermal expansion, Debye temperature, melting point, and Grüneisen parameters. High-accuracy, efficient calculations based on density

functional theory (DFT) are at the point of providing an alternative to experimental determination of elastic constants, especially for complicated crystal structures. This is evidenced by a large number of papers on *ab initio* calculations of SOECs [1–7] in the literature. In all these works, only selected materials, *i.e.*, exhibiting a particular lattice type, have been investigated. More systematic work on SOECs has been presented in Refs. [8,9], which focus on the elastic properties of ceramic materials. Recently, more systematic methodological approaches for calculating the SOECs have been pursued in Refs. [10,11] using the computer packages CRYSTAL and VASP, respectively. In the present work, we introduce ElaStic which is a tool that allows for the *ab initio* calculation of SOECs using two approaches based on the numerical differentiation of either the total energy or the physical stress of a crystal as a function of the imposed strain. The current implementation of ElaStic is interfaced with the computer packages *exciting*, WIEN2k, and Quantum ESPRESSO, all of them based on DFT [12,13]. Extensions of ElaStic to interface it with other DFT codes will be straightforward. Furthermore, we introduce a procedure which allows for reducing numerical errors appearing in the evaluation of elastic constants.

\* Correspondence to: Institut für Physik, Humboldt-Universität zu Berlin, Newtonstr. 15, D-12489 Berlin, Germany. Tel.: +49 17638828803; fax: +49 3020966361.

E-mail address: [rostam@physik.hu-berlin.de](mailto:rostam@physik.hu-berlin.de) (R. Golesorkhtabar).

<sup>1</sup> Present address: Institut für Physik, Humboldt-Universität zu Berlin, Newtonstr. 15, D-12489 Berlin, Germany.

<sup>2</sup> Present address: Institut für Physik, Karl-Franzens-Universität Graz, Universitätsplatz 5, 8010 Graz, Austria.

In order to show the potential and accuracy of `ElaStic`, we have applied this tool to a set of prototype materials covering all crystal families and different types of atomic bonds (*i.e.*, covalent, ionic, and intermetallic). Note that extension to van der Waals bonded systems is straightforward as van der Waals density functionals [14] can be used in combination with all major DFT codes [15]. As typical representatives of this bonding are molecular crystals with large unit cells, we, however, do not show such an example here.

The outline of the paper is as follows: In Section 2, we introduce the SOECs from a theoretical point of view. The algorithm that is used by `ElaStic` is presented in Section 3. In Section 4, the influence of some numerical parameters on the fitting procedure is demonstrated with the help of a simple model. The application of the same approach to realistic systems is discussed in Section 5. Computational details and results for several prototype materials are presented in Sections 6 and 7, respectively.

## 2. Methodology

Elastic properties are conventionally described within the Lagrangian theory of elasticity [16]. Within this theory, a solid can be viewed as a homogeneous and anisotropic elastic medium. Therefore, strain and stress are homogeneous and are represented in terms of symmetric second-rank tensors (indicated by the bold font below). The Lagrangian strain,  $\boldsymbol{\eta}$ , and the stress,  $\boldsymbol{\tau}$ , are defined as

$$\boldsymbol{\eta} = \boldsymbol{\epsilon} + \frac{1}{2}\boldsymbol{\epsilon}^2, \quad (1)$$

$$\boldsymbol{\tau} = \det(\mathbf{1} + \boldsymbol{\epsilon}) (\mathbf{1} + \boldsymbol{\epsilon})^{-1} \cdot \boldsymbol{\sigma} \cdot (\mathbf{1} + \boldsymbol{\epsilon})^{-1}, \quad (2)$$

where the dot ( $\cdot$ ) indicates a tensor product;  $\boldsymbol{\epsilon}$  is the physical strain tensor, transforming a position vector  $\mathbf{r}$  to  $(\mathbf{1} + \boldsymbol{\epsilon}) \cdot \mathbf{r}$  in Cartesian coordinates; and  $\boldsymbol{\sigma}$  is the physical stress tensor defined by differentiation of the total energy,  $E$ , as

$$\boldsymbol{\sigma} = \frac{1}{V} \frac{\partial^2 E}{\partial \boldsymbol{\epsilon}^2}, \quad (3)$$

where  $V$  is the volume of the crystal. Within the linear regime, the Lagrangian stress and strain are related by the generalized Hooke's law

$$\tau_{ij} = \sum_{k,l=1}^3 c_{ijkl} \eta_{kl}. \quad (4)$$

Here, the coefficients  $c_{ijkl}$  are the elastic stiffness constants of the crystal and represent the tensor components of the forth-rank stiffness (or elasticity) tensor,  $\mathbf{c}$ . Eq. (4) can be inverted to the form

$$\eta_{ij} = \sum_{k,l=1}^3 s_{ijkl} \tau_{kl}, \quad (5)$$

where  $s_{ijkl}$  are the components of the compliance tensor,  $\mathbf{s}$ .

An alternative approach to elasticity is obtained by expressing the total energy of a crystal in terms of a power series of the strain,  $\boldsymbol{\eta}$ , as

$$E(\boldsymbol{\eta}) = E(0) + V_0 \sum_{i,j=1}^3 \tau_{ij}^{(0)} \eta_{ij} + \frac{V_0}{2!} \sum_{i,j,k,l=1}^3 c_{ijkl} \eta_{ij} \eta_{kl} + \dots, \quad (6)$$

where  $E(0)$  and  $V_0$  are the energy and volume of the reference structure (usually the equilibrium one), respectively. In order to simplify the expressions, it is convenient to use the Voigt notation,

in which each pair of Cartesian indices  $ij$  are replaced by a single index  $\alpha$ , according to

$$\begin{array}{l} ij \\ \alpha \end{array} \begin{array}{cccccc} 11 & 22 & 33 & 23 & 13 & 12 \\ 1 & 2 & 3 & 4 & 5 & 6 \end{array}.$$

Using this notation, Eq. (4) reads

$$\tau_\alpha = \sum_\beta c_{\alpha\beta} \eta_\beta, \quad (7)$$

where the sum runs implicitly on the Voigt components from 1 to 6. In a similar way, Eq. (6) becomes

$$E(\boldsymbol{\eta}) = E(0) + V_0 \sum_\alpha \tau_\alpha^{(0)} \eta_\alpha + \frac{V_0}{2!} \sum_{\alpha,\beta} c_{\alpha\beta} \eta_\alpha \eta_\beta + \dots. \quad (8)$$

If the reference structure is chosen to be the equilibrium one, all  $\tau_\alpha^{(0)}$  vanish, because in equilibrium the crystal is stress free.

According to Eqs. (7) and (8), respectively, the elastic constant  $c_{\alpha\beta}$  can be derived using two equivalent expressions

$$c_{\alpha\beta} = \left. \frac{\partial \tau_\alpha}{\partial \eta_\beta} \right|_{\eta=0} \quad (9)$$

and

$$c_{\alpha\beta} = \left. \frac{1}{V_0} \frac{\partial^2 E}{\partial \eta_\alpha \partial \eta_\beta} \right|_{\eta=0}. \quad (10)$$

These derivatives are calculated at the reference configuration ( $\boldsymbol{\eta} = 0$ ). First-principles calculation of the SOECs with the use of Eq. (9) have been performed first by Nielsen and Martin [17,18]. This approach is preferred when the calculation of the stress tensor is included in the DFT package. The available codes in which this kind of calculation is implemented, actually obtain the physical stress  $\boldsymbol{\sigma}$ , rather than the Lagrangian stress  $\boldsymbol{\tau}$ . Under this condition, Eq. (2) must be used to convert  $\boldsymbol{\sigma}$  to  $\boldsymbol{\tau}$ . In the following, we denominate the procedure based on stress calculations, *i.e.*, on Eq. (9), as “*stress approach*”. Correspondingly, the calculation of the SOECs using Eq. (10) will be referred to as “*energy approach*”. In both approaches, one first chooses a deformation type, *i.e.*, an appropriate strain vector (in the Voigt notation), *e.g.*,  $\boldsymbol{\eta} = (\eta, \eta, \eta, 0, 0, 0)$ , with values of  $\eta$  taken around the origin. Then, numerical derivatives are taken of the resulting energy or stress curves in dependence of the parameter  $\eta$ . This procedure yields a linear combination of SOECs. If the recipe is repeated for a properly chosen set of deformation types, the values of single SOECs can be achieved solving the resulting equations.

## 3. Calculation of second-order elastic constants

The standard fully-automated procedure for the calculation of SOECs with `ElaStic` for an arbitrary crystal is described in the following. As a starting point, we assume that the geometry of the crystal has been optimized for both, cell parameters and atomic positions, such that the equilibrium configuration is used as reference system. In this case, all the curves representing the energy as a function of strain have a minimum at zero strain. Correspondingly, the stress–strain curves are passing through the origin. The flowchart of `ElaStic` as shown in Fig. 1, displays the single steps of the procedure:

- *Specify the DFT code*

One of the available computer packages `exciting`, `WIEN2k`, and `Quantum ESPRESSO` is chosen for performing the DFT calculations. (The addition of interfaces with other *ab initio* DFT codes to `ElaStic` is straightforward.)

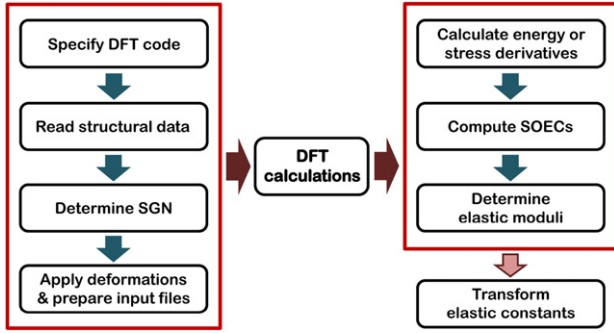


Fig. 1. Flowchart of the algorithm used in the ElaStic tool.

- **Read the structure file**

An input file containing information about the structure (crystal lattice, atomic positions, etc.) should be provided. For this purpose, ElaStic requires the input file which is used by the selected DFT code for a calculation at the equilibrium structure with relaxed atomic positions. The structural data contained in the input file are read by ElaStic.

- **Determine the space-group number**

In order to fully characterize the system crystallographically, the space-group number (SGN) must be determined. This is performed by the code SGROUP [19]. A classification of the different crystal structures including the corresponding number of independent SOECs is given in Table 1.

- **Deform the crystal and prepare input files**

From the knowledge of the SGN, a set of deformation types will be specified. All deformation types utilized in ElaStic are shown in Tables 2 and 3 for the energy and stress approach, respectively. Two input values, the maximum absolute value for the Lagrangian strain,  $\eta_{\max}$ , and the number of distorted structures with strain values between  $-\eta_{\max}$  and  $\eta_{\max}$ , should be provided by the user at this stage. Then, input files for the chosen DFT code are created for each deformed structure.

- **Perform *ab initio* calculations**

The energy or stress for the set of distorted structures created at the previous step is calculated by the selected DFT code. For each deformed structure, the internal degrees of freedom are optimized.

- **Calculate derivatives: Best polynomial fit**

A polynomial fitting procedure is applied to calculate the second (first) derivative at equilibrium of the energy (stress) with respect to the Lagrangian strain. It will be discussed in Section 4 how the order of the polynomial fit and the distortion range can influence the values of the SOECs.

- **Calculate SOECs: Least-squares fit**

The quadratic (linear) coefficients of the best fitting polynomial achieved at the previous step can be expressed as linear combination of the SOECs. This procedure is repeated for a number of different deformation types, thus obtaining a set of linear equations which is (possibly) redundant in terms of the variables, *i.e.*, of the SOECs. This set of linear equations is solved by a least-square fit.

- **Calculate elastic moduli**

Appropriate averaging procedures can determine isotropic elastic constants such as the bulk, shear, and Young modulus. In ElaStic, three of the most widely used averaging approaches are implemented. While in the Voigt [20] approach a uniform strain is assumed, the Reuss [21] procedure is valid for the case of uniform stress. The resulting Voigt and Reuss moduli are expressed in terms of the stiffness constants,  $c_{ij}$ , and compliances,

$s_{ij}$ , respectively. In particular, the bulk and shear modulus in the Voigt approach are

$$B_V = \frac{1}{9} [(c_{11} + c_{22} + c_{33}) + 2(c_{12} + c_{13} + c_{23})], \quad (11)$$

$$G_V = \frac{1}{15} [(c_{11} + c_{22} + c_{33}) - (c_{12} + c_{13} + c_{23}) + 3(c_{44} + c_{55} + c_{66})]. \quad (12)$$

The corresponding expressions for the Reuss procedure are

$$B_R = [(s_{11} + s_{22} + s_{33}) + 2(s_{12} + s_{13} + s_{23})]^{-1}, \quad (13)$$

$$G_R = 15 [4(s_{11} + s_{22} + s_{33}) - (s_{12} + s_{13} + s_{23}) + 3(s_{44} + s_{55} + s_{66})]^{-1}. \quad (14)$$

Hill [22,23] has shown that the Voigt and Reuss elastic moduli are the strict upper and lower bound, respectively. Thus, the Hill-averaged bulk and shear moduli can be determined from these upper and lower limits as

$$G_H = \frac{1}{2}(G_V + G_R), \quad (15)$$

$$B_H = \frac{1}{2}(B_V + B_R). \quad (16)$$

For all the averaged procedures presented here, the Young modulus,  $E$ , and the Poisson ratio,  $\nu$ , can be obtained in connection with the bulk modulus,  $B$ , and the shear modulus,  $G$ , as

$$E = \frac{9BG}{3B + G}, \quad (17)$$

$$\nu = \frac{3B - 2G}{2(3B + G)}. \quad (18)$$

- **Post-processing: Transform elastic tensors**

ElaStic can also be used to perform some post-processing of the obtained results. For example, ElaStic includes a tool that converts the elastic-constants tensor from one reference system with Cartesian coordinates  $x_i$  to another one with transformed coordinates  $X_i = \sum_{j=1}^3 a_{ij}x_j$ , where  $a_{ij}$  is the cosine of the angle between the directions of  $X_i$  and  $x_j$ . The transformation for the components of the elastic-constant tensor is given by

$$C_{ijkl} = \sum_{m,n,p,q=1}^3 a_{im} a_{jn} a_{kp} a_{lq} c_{mnpq}, \quad (19)$$

where  $c_{mnpq}$  ( $C_{ijkl}$ ) are the second-order elastic constants in the old (new) Cartesian coordinates.

#### 4. Accuracy and numerical differentiation

The numerical accuracy of the elastic-constant calculations described in the last sections is strongly correlated with the numerical differentiation needed for the evaluation of Eqs. (9) and (10). In fact, we deal with a function (energy or stress) which is calculated only for a finite set of strain values. The evaluation of the numerical derivative of a such a function is a non trivial issue. Several parameters play an important role, like the number and range of data points included in the fit and the kind of procedure used for the differentiation. In addition, computed DFT data are obtained up to a certain accuracy. In order to keep all these parameters under control and to estimate the impact of numerical uncertainties of energies and stresses, we have developed a special fitting procedure. It will be illustrated in the next section for a simple model where we treat the numerical error by adding random noise to the energy (stress) values. Then, the application of this procedure will

**Table 1**  
Classification of crystal families and systems. Centering type, Laue group, Hermann–Mauguin point-group symbols, and space-group numbers (SGN) are provided together with the number of independent SOECs. In the last column, prototype materials are shown.

Crystal family	Crystal system	Centering type(s)	Laue group	Point group classes	SGN	No. of SOECs	Prototype material(s)
Cubic	Cubic	$P, F, I$	$C_1$	$432, 4\bar{3}m, \frac{4}{m}\bar{3}\frac{2}{m}$	207–230	3	C, Al, CsCl
			$C_{II}$	$23, \frac{2}{m}\bar{3}$	195–206		
Hexagonal	Hexagonal	$P$	$H_1$	$622, 6mm, \bar{6}2m, \frac{6}{m}\frac{2}{m}\frac{2}{m}$	177–194	5	Ti, TiB <sub>2</sub>
			$H_{II}$	$6, \bar{6}, \frac{6}{m}$	168–176		
	Trigonal	$P, R$	$R_1$	$32, 3m, \bar{3}\frac{2}{m}$	149–167	6	Al <sub>2</sub> O <sub>3</sub>
Tetragonal	Tetragonal	$P, I$	$R_{II}$	$3, \bar{3}$	143–148	7	CaMg(CO <sub>3</sub> ) <sub>2</sub>
			$T_1$	$422, 4mm, \bar{4}2m, \frac{4}{m}\frac{2}{m}\frac{2}{m}$	89–142	6	MgF <sub>2</sub>
			$T_{II}$	$4, \bar{4}, \frac{4}{m}$	75–88	7	CaMoO <sub>4</sub>
Orthorhombic	Orthorhombic	$P, C, F, I$	O	$222, mm2, \frac{2}{m}\frac{2}{m}\frac{2}{m}$	16–74	9	TiSi <sub>2</sub>
Monoclinic	Monoclinic	$P, C$	M	$m, 2, \frac{2}{m}$	3–15	13	ZrO <sub>2</sub>
Triclinic	Triclinic	$P$	N	$1, \bar{1}$	1 and 2	21	TiSi <sub>2</sub>

**Table 2**  
Deformation types, expressed in the Voigt notation, that are used by ElaStic in the energy approach. Here, the generic (*i*-th) strain tensor is represented as a vector  $\eta^{(i)} = (\eta_1, \eta_2, \eta_3, \eta_4, \eta_5, \eta_6)$ .

$\eta^{(i)}$	$\eta_1$	$\eta_2$	$\eta_3$	$\eta_4$	$\eta_5$	$\eta_6$
$\eta^{(1)}$	$\eta$	$\eta$	$\eta$	0	0	0
$\eta^{(2)}$	$\eta$	0	0	0	0	0
$\eta^{(3)}$	0	$\eta$	0	0	0	0
$\eta^{(4)}$	0	0	$\eta$	0	0	0
$\eta^{(5)}$	0	0	0	$2\eta$	0	0
$\eta^{(6)}$	0	0	0	0	$2\eta$	0
$\eta^{(7)}$	0	0	0	0	0	$2\eta$
$\eta^{(8)}$	$\eta$	$\eta$	0	0	0	0
$\eta^{(9)}$	$\eta$	0	$\eta$	0	0	0
$\eta^{(10)}$	$\eta$	0	0	$2\eta$	0	0
$\eta^{(11)}$	$\eta$	0	0	0	$2\eta$	0
$\eta^{(12)}$	$\eta$	0	0	0	0	$2\eta$
$\eta^{(13)}$	0	$\eta$	$\eta$	0	0	0
$\eta^{(14)}$	0	$\eta$	0	$2\eta$	0	0
$\eta^{(15)}$	0	$\eta$	0	0	$2\eta$	0
$\eta^{(16)}$	0	$\eta$	0	0	0	$2\eta$
$\eta^{(17)}$	0	0	$\eta$	$2\eta$	0	0
$\eta^{(18)}$	0	0	$\eta$	0	$2\eta$	0
$\eta^{(19)}$	0	0	$\eta$	0	0	$2\eta$
$\eta^{(20)}$	0	0	0	$2\eta$	$2\eta$	0
$\eta^{(21)}$	0	0	0	$2\eta$	0	$2\eta$
$\eta^{(22)}$	0	0	0	0	$2\eta$	$2\eta$
$\eta^{(23)}$	0	0	0	$2\eta$	$2\eta$	$2\eta$
$\eta^{(24)}$	$-\eta$	$\frac{1}{2}\eta$	$\frac{1}{2}\eta$	0	0	0
$\eta^{(25)}$	$\frac{1}{2}\eta$	$-\eta$	$\frac{1}{2}\eta$	0	0	0
$\eta^{(26)}$	$\frac{1}{2}\eta$	$\frac{1}{2}\eta$	$-\eta$	0	0	0
$\eta^{(27)}$	$\eta$	$-\eta$	0	0	0	0
$\eta^{(28)}$	$\eta$	$-\eta$	0	0	0	$2\eta$
$\eta^{(29)}$	0	$\eta$	$-\eta$	0	0	$2\eta$

**Table 3**  
Same as Table 2 for the stress approach. The choice of deformation types is made according to Ref. [11].

$\tilde{\eta}_i$	$\eta_1$	$\eta_2$	$\eta_3$	$\eta_4$	$\eta_5$	$\eta_6$
$\tilde{\eta}^{(1)}$	$\eta$	$2\eta$	$3\eta$	$4\eta$	$5\eta$	$6\eta$
$\tilde{\eta}^{(2)}$	$-2\eta$	$\eta$	$4\eta$	$-3\eta$	$6\eta$	$-5\eta$
$\tilde{\eta}^{(3)}$	$3\eta$	$-5\eta$	$-\eta$	$6\eta$	$2\eta$	$-4\eta$
$\tilde{\eta}^{(4)}$	$-4\eta$	$-6\eta$	$5\eta$	$\eta$	$-3\eta$	$2\eta$
$\tilde{\eta}^{(5)}$	$5\eta$	$4\eta$	$6\eta$	$-2\eta$	$-\eta$	$-3\eta$
$\tilde{\eta}^{(6)}$	$-6\eta$	$3\eta$	$-2\eta$	$5\eta$	$-4\eta$	$\eta$

be validated for some prototypical real materials. Here, only results for the energy approach are shown, but the extension to the stress approach is straightforward.

#### 4.1. An analytical example

In the following, we demonstrate the reliability of numerical energy derivatives by a simple test case. We assume that the energy vs. strain relationship is known and is *exactly* given as a polynomial function in the strain  $\eta$  of a certain degree. In this example, without loss of generality, we consider a polynomial of order 6,

$$E(\eta) = \sum_{i=1}^6 A_i \eta^i, \quad (20)$$

with known coefficients  $A_i$ . In particular, the coefficient  $A_2$  is set to  $A_2 = 100$  (in arbitrary units). Obviously, in this special case, the differentiation can be performed analytically; nevertheless, we calculate the second-order derivative with standard numerical techniques. Therefore, we generate a set of 51 equally-spaced strain points with symmetric distribution around the origin in the range  $\eta \in [-0.1, 0.1]$  and calculate the energy values using Eq. (20). A polynomial fit yields the exact value of  $A_2$  if the order of the polynomial is equal to or larger than 6. The procedure can be repeated by taking into account only strain points in the range  $\eta \in [-\eta_{\max}, \eta_{\max}]$  for different values of  $\eta_{\max}$  (keeping the strain-point density fixed). The energy as a function of  $\eta$  calculated from Eq. (20), and the value of  $A_2$  as a function of  $\eta_{\max}$  are shown in the left and right top panels of Fig. 2, respectively. Due to the choice of a symmetric distribution of strain points around the origin, the fitting polynomials of order  $n$  and  $n + 1$  with even  $n$  provide the same value of  $A_2$ , as can be seen in the figure. The results for the quadratic polynomial fit are close to the correct value only for  $\eta_{\max} < 0.01$ . The fourth order fit provides the correct result for  $\eta_{\max} < 0.35$ , while the sixth order can be used for any value of  $\eta_{\max}$ .

The example used here is very simple and somehow trivial. However, the situation is different considering that the values of the function  $E(\eta)$  are not known exactly, but include some intrinsic numerical error introduced by calculating DFT total energies. We simulate the effect of such errors by adding a random noise of given amplitude to the polynomial function in Eq. (20), as given by

$$\tilde{E}_\Delta(\eta) = E(\eta) + \xi \Delta (E_{\max} - E_{\min}), \quad (21)$$

where  $E_{\max}$  and  $E_{\min}$  are the maximum and minimum of the function  $E(\eta)$  in the range  $\eta \in [-0.1, 0.1]$ , and  $\xi$  is a randomly generated number in the range  $\xi \in [-1, 1]$ .

The results for  $\Delta = 0.005$  and  $\Delta = 0.02$  are shown in the middle and lower right panels of Fig. 2, respectively. The main effect of the noise is to generate deviations from the unperturbed curves, strongly depending on the order of the polynomial fit,  $\eta_{\max}$ , and the noise amplitude. Analysis of the two lower panels identifies two different trends in dependence of the fitting order:

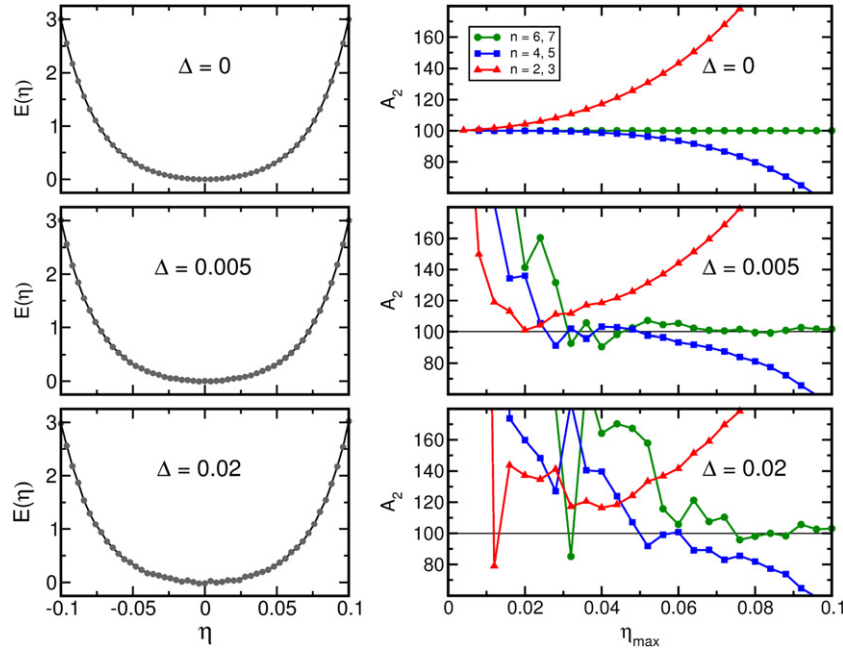


**Fig. 2.** Energy as a function of strain  $\eta$  calculated from Eq. (21) for different amplitudes of noise,  $\Delta = 0, 0.005$ , and  $0.02$ , respectively (left) and the corresponding coefficient  $A_2$  as obtained from different polynomial fits (right).

- (i) For small deformations, the best results for the derivative are obtained by using low-order polynomial fit. The same holds true if only a few data points are taken into account for the fit. The better values for the derivative arise in this case from the fact that the noise is partially averaged out using low-order polynomials, while high-order ones follow the noise much more, developing unphysical wiggles and, thus, yielding completely wrong coefficients.
- (ii) The results obtained for large deformations are very close to the correct value for high-order polynomial fit, in particular, in the strain regions where the curves in the right panel of Fig. 2 are flat.

From the previous analysis, we conclude that, for a fixed order of the polynomial fit, the *correct* value of  $A_2$  is best reproduced in a region of  $\eta_{\max}$  that is characterized by a *plateau* of the displayed curves. For instance, for the largest noise amplitude (bottom right), in the range  $\eta_{\max} > 0.08$  only the sixth order polynomial fit gives *reasonable* results for the coefficient  $A_2$ . Considering that low-order polynomial fit gives good results only for small values of  $\eta_{\max}$ , the application of a high-order polynomial fit is thus preferable. This means, in turn, that large values of  $\eta_{\max}$  and a considerable number of strain points should be used in order to identify the plateaus.

These results allow to establish a general criterion for finding the best numerical derivative of a function. In practice, one needs to identify the flat regions (plateaus), which typically move to higher values of  $\eta_{\max}$  when applying a higher-order polynomial fit.

In addition to the above analysis, the simple model introduced before can be used to investigate the intrinsic accuracy of the energy values. This can be done with the help of a cross-validation (CV) method [24–26]. In general, the CV technique allows for optimization of the fitting procedure performed on a sample of statistical data. Here we apply the leave-one-out cross-validation score.

In our simple example, the statistical sample consists of  $N$  pairs of the type  $(\eta_i, E_i)$ . The CV error of a polynomial fit of order  $n$  can be calculated as

$$\delta_{CV}^{(n)} = \sqrt{\frac{1}{N} \sum_{i=1}^N [E_i - p^{(n)}(\eta_i)]^2}, \quad (22)$$

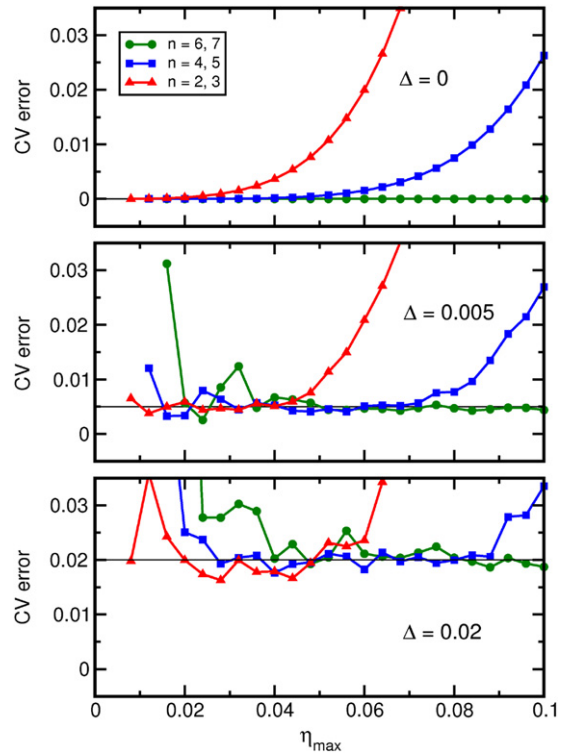


**Fig. 3.** The cross-validation (CV) error defined in Eq. (22) as a function of  $\eta_{\max}$  for different values of the maximum noise amplitude for the simple model discussed in the text. The upper, middle, and lower panel illustrate the result for  $\Delta = 0$  (no noise),  $0.005$  (low noise), and  $0.02$  (high noise), respectively.

where  $p^{(n)}(\eta_i)$  is the value at  $\eta_i$  of the polynomial function of order  $n$  which has been obtained by applying the polynomial fit order  $n$  to  $N - 1$  points of the sample, *i.e.*, excluding the pair  $(\eta_i, E_i)$ .

The CV error defined in Eq. (22) as a function of  $\eta_{\max}$  for different orders of the polynomial fit is shown in Fig. 3. The behavior of the different curves is similar to the corresponding ones in Fig. 2.

**Table 4**

List of deformation types used in ELaStic for the different Laue groups in the energy approach. The number of deformation types, equal to the number of independent SOECs, is denoted by  $N_{DT}$ . Deformation types are labeled according to Table 2.

Laue group	$N_{DT}$	Deformation types
$C_{1,II}$	3	$\eta^{(1)}, \eta^{(8)}, \eta^{(23)}$
$H_{1,II}$	5	$\eta^{(1)}, \eta^{(3)}, \eta^{(4)}, \eta^{(17)}, \eta^{(26)}$
$R_I$	6	$\eta^{(1)}, \eta^{(2)}, \eta^{(4)}, \eta^{(5)}, \eta^{(8)}, \eta^{(10)}$
$R_{II}$	7	$\eta^{(1)}, \eta^{(2)}, \eta^{(4)}, \eta^{(5)}, \eta^{(8)}, \eta^{(10)}, \eta^{(11)}$
$T_I$	6	$\eta^{(1)}, \eta^{(4)}, \eta^{(5)}, \eta^{(7)}, \eta^{(26)}, \eta^{(27)}$
$T_{II}$	7	$\eta^{(1)}, \eta^{(4)}, \eta^{(5)}, \eta^{(7)}, \eta^{(26)}, \eta^{(27)}, \eta^{(28)}$
O	9	$\eta^{(1)}, \eta^{(3)}, \eta^{(4)}, \eta^{(5)}, \eta^{(6)}, \eta^{(7)}, \eta^{(25)}, \eta^{(26)}, \eta^{(27)}$
M	13	$\eta^{(1)}, \eta^{(3)}, \eta^{(4)}, \eta^{(5)}, \eta^{(6)}, \eta^{(7)}, \eta^{(12)}, \eta^{(20)}, \eta^{(24)}, \eta^{(25)}, \eta^{(27)}, \eta^{(28)}, \eta^{(29)}$
N	21	$\eta^{(2)}, \eta^{(3)}, \eta^{(4)}, \eta^{(5)}, \eta^{(6)}, \eta^{(7)}, \eta^{(8)}, \eta^{(9)}, \eta^{(10)}, \eta^{(11)}, \eta^{(12)}, \eta^{(13)}, \eta^{(14)}, \eta^{(15)}, \eta^{(16)}, \eta^{(17)}, \eta^{(18)}, \eta^{(19)}, \eta^{(20)}, \eta^{(21)}, \eta^{(22)}$

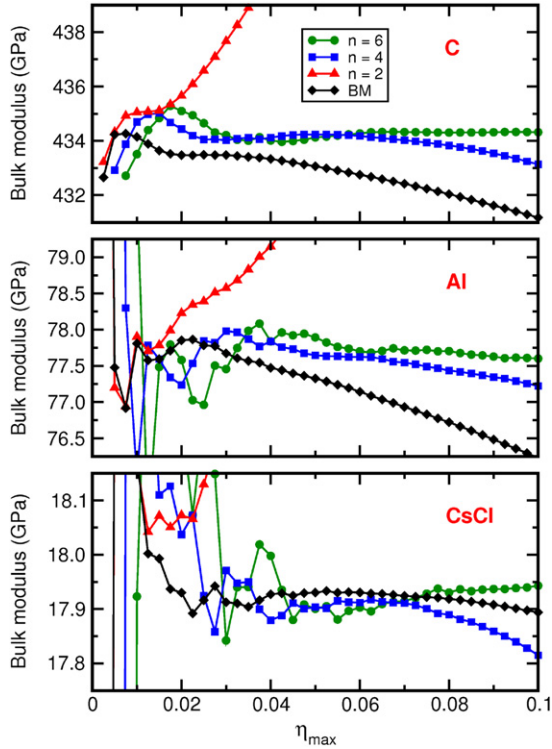


**Fig. 4.** Bulk modulus as a function of the maximum absolute value of deformation,  $\eta_{\max}$ , for three cubic materials: diamond (upper panel), fcc Al (middle panel), and sc CsCl (lower panel). The calculations have been performed using the WIEN2k code.

However, in this case, each plateau value gives an estimation of the maximum noise amplitude. Therefore, for real materials, this result can be used to check the numerical accuracy of the energy obtained by the *ab initio* calculation. In fact, if a too large plateau value is found, the accuracy of the DFT computations should be probably improved.

#### 4.2. Test examples for real materials

The method illustrated in the previous section can also be applied to real systems, under the assumption that the errors in the calculated DFT energies are statistically independent. Here we investigate the bulk modulus considering the three cubic materials diamond, Al, and CsCl. They are representative systems which can be classified from the elastic point of view as hard, medium, and soft materials, respectively.

In Fig. 4, we show the result of WIEN2k calculations as a function of  $\eta_{\max}$  and for different orders of the polynomial used in the fitting procedure. As explained in the previous section, only even values of the polynomial order are significant. The deformation type which is used here is a uniform volume change. In addition

to the results of the polynomial fit, Fig. 4 also displays the value of the bulk modulus as obtained using the equation-of-state fitting procedure proposed by Birch and Murnaghan (BM) [27]. The trends observed for the polynomial fits in Fig. 4 are the same as for the noisy curves of the simple model (right panel of Fig. 2). The converged values of the bulk modulus for the polynomial and the equation-of-state fit, as denoted by the flat part of curves in Fig. 4, are comparable. As the equation-of-state fit is limited in its application, ELaStic has implemented the more general polynomial-fit procedure. The choice of the optimal fitting parameters depends on both the material and the applied deformation type. For most of the prototype materials reported in Section 7, results have been obtained using a sixth-order polynomial fit with values of  $\eta_{\max}$  in the range  $\eta_{\max} \in [0.05, 0.08]$ .

#### 5. Choice of deformations

A prominent role in ensuring high accuracy in the calculation of SOECs is played by the choice of the deformation types selected for each crystal structure. The list of the deformation types used in the ELaStic tool are presented in Tables 4 and 5 for the energy and stress approach, respectively. In ELaStic different criteria are followed for this choice depending on the specific kind of approach.

In the stress approach, the deformation types are defined according to Ref. [11]. Here, deformations corresponding to the so-called universal linear-independent coupling strains [11] are used. Although the corresponding deformed structures exhibit very low symmetry, this choice requires only a small number of deformation types.

A different criterion is followed in the energy approach. We have chosen a set of deformation types where the symmetry of the unperturbed system is least reduced by applying strain. There are two reasons for this: The first one is to minimize the computational effort as DFT codes can make use of symmetry. Second, low symmetry may also lead to very slow convergence with respect to computational parameters as has been reported in the literature [28].

The choice of too large values for  $\eta_{\max}$  should be avoided due to the possible onset of a phase transition. For instance, this happens in the calculation of  $c_{44}$  of cubic diamond when applying the  $\eta^{(23)}$  deformation type. The total energy as a function of strain for this case is shown in Fig. 5. It exhibits a kink at  $\eta = 0.08$  related to the onset of a phase transition from the (deformed) diamond structure to a lamellar rhombohedral system where the carbon sheets are oriented orthogonally to the (1, 1, 1) direction of the cubic diamond structure.

#### 6. Computational details

The energies and stresses of the distorted structures are calculated using the DFT codes *exciting*, WIEN2k, and Quantum ESPRESSO. In all these codes, the Kohn–Sham (KS) equations of DFT [13] is solved self-consistently. However, they differ in

**Table 5**

List of deformation types used in ELaStic for the different Laue groups in the stress approach. The number of deformation types is denoted by  $N_{DT}$ . Deformation types are labeled according to Table 3.

Laue group	$N_{DT}$	Deformation types
$C_{1,II}$	1	$\tilde{\eta}^{(1)}$
$H_{1,II}$	2	$\tilde{\eta}^{(1)}, \tilde{\eta}^{(3)}$
$R_{1,II}$	2	$\tilde{\eta}^{(1)}, \tilde{\eta}^{(3)}$
$T_{1,II}$	2	$\tilde{\eta}^{(1)}, \tilde{\eta}^{(3)}$
O	3	$\tilde{\eta}^{(1)}, \tilde{\eta}^{(3)}, \tilde{\eta}^{(5)}$
M	5	$\tilde{\eta}^{(1)}, \tilde{\eta}^{(2)}, \tilde{\eta}^{(3)}, \tilde{\eta}^{(4)}, \tilde{\eta}^{(5)}$
N	6	$\tilde{\eta}^{(1)}, \tilde{\eta}^{(2)}, \tilde{\eta}^{(3)}, \tilde{\eta}^{(4)}, \tilde{\eta}^{(5)}, \tilde{\eta}^{(6)}$

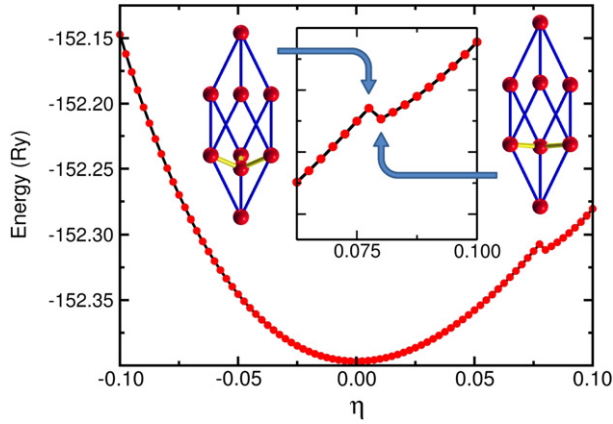


**Fig. 5.** Total energy of the deformed diamond structure by applying the  $\eta^{(23)}$  deformation type. At  $\eta = 0.08$ , the kink indicates the transition to a different rhombohedral structure.

**Table 6**

Computational parameters used for lattice optimization and elastic-constant calculations with `exciting` and WIEN2k. Smearing values ( $\sigma_{smear}$ ) are given in Ry, muffin-tin radii ( $R_{MT}$ ) are in atomic units.

Material	Atom	$R_{MT}$	$R_{MT}K_{max}$	<b>k</b> -mesh	$\sigma_{smear}$
C	C	1.15	8.0	$15 \times 15 \times 15$	–
Al	Al	2.00	9.0	$36 \times 36 \times 36$	0.025
CsCl	Cs	2.00	9.0	$15 \times 15 \times 15$	–
	Cl	2.00			
Ti	Ti	2.00	8.0	$16 \times 16 \times 9$	0.010
TiB <sub>2</sub>	Ti	2.23	9.0	$15 \times 15 \times 12$	–
	B	1.54			
Al <sub>2</sub> O <sub>3</sub>	Al	1.64	8.0	$8 \times 8 \times 8$	–
	O	1.64			
MgF <sub>2</sub>	Mg	1.80	8.0	$10 \times 10 \times 16$	–
	F	1.40			
CaMoO <sub>4</sub>	Ca	1.60	8.0	$8 \times 8 \times 8$	0.010
	Mo	1.60			
	O	1.50			
TiSi <sub>2</sub>	Ti	2.10	8.5	$8 \times 8 \times 8$	–
	Si	1.50			
ZrO <sub>2</sub>	Zr	1.75	8.0	$7 \times 8 \times 7$	–
	O	1.55			
TiSi <sub>2</sub>	Ti	2.00	8.5	$14 \times 12 \times 14$	–
	Si	2.00			

the choice of the basis set representing the KS orbitals. While `exciting` and WIEN2k are based on the full-potential (linearized) augmented plane-wave and local-orbitals (FP-(L)APW+lo) method, the Quantum ESPRESSO software package relies on a plane-wave

**Table 7**

Computational parameters used for lattice optimization and elastic-constant calculations with the Quantum ESPRESSO code. Kinetic-energy cutoffs ( $E_{cut}$ ) and smearing values ( $\sigma_{smear}$ ) are given in Ry.

Material	$E_{cut}^{(wfc)}$	$E_{cut}^{(rho)}$	<b>k</b> -mesh	$\sigma_{smear}$
C	80	480	$15 \times 15 \times 15$	–
Al	80	800	$36 \times 36 \times 36$	0.025
Ti	80	800	$16 \times 16 \times 9$	0.010
TiB <sub>2</sub>	100	1000	$15 \times 15 \times 12$	–
Al <sub>2</sub> O <sub>3</sub>	80	800	$8 \times 8 \times 8$	–
MgF <sub>2</sub>	80	800	$10 \times 10 \times 16$	–
CaMoO <sub>4</sub>	80	800	$8 \times 8 \times 8$	0.010
TiSi <sub>2</sub>	80	800	$8 \times 8 \times 8$	0.010
ZrO <sub>2</sub>	80	800	$7 \times 8 \times 7$	–

basis set and the pseudo-potential approximation. In the most recent implementations, the direct calculation of the stress tensor is available only for the Quantum ESPRESSO package; therefore all our results for the stress approach have been obtained by using this code.

First-principles calculations have been performed for a set of materials. At least one representative crystal for each crystal system has been chosen. Extensive tests for each considered crystal have been carried out to ensure that the calculated properties are converged within a certain accuracy, with respect to all computational parameters, e.g., the **k**-point mesh, the basis set size, and the expansion of the charge density. The main computational parameters which have been used to perform the calculations presented in this work are shown in Tables 6 (for `exciting` and WIEN2k) and 7 (for Quantum ESPRESSO).

In all calculations exchange–correlation effects have been treated within the generalized-gradient approximation (GGA) with the PBE [29] functional. The accuracy of the PBE functional in providing results for elastic constants has been already shown in the literature [1–7]. Exceptionally, for the calculation of CsCl we have used the PBEsol [30] exchange–correlation functional which allows for a better description of the inter-atomic bonding, in particular for systems which are characterized by small values of SOECs, such as CsCl. In fact, the agreement with experimental data for the elastic constants is improved from about 21% deviation to less than 2% using PBEsol instead of PBE.

For the integration over the Brillouin zone, we have employed the improved tetrahedron [31] method as well as summations over special points within the Monkhorst–Pack [32] scheme. For metallic systems, the Gaussian-smearing technique [33] has been applied. For lattice relaxations, convergence has been achieved for residual forces and stresses lower than 0.1 mRy/bohr and 50 MPa, respectively.

## 7. Results

In this section, we present the results for the SOECs obtained by the ELaStic code. Our main goal consists in showing the reliability of results and used procedures. We are not particularly aiming at matching experimental values, which could be obtained under conditions which are different from the ones considered for the calculations. For instance, theoretical data obtained using DFT should be interpreted only as  $T = 0$  K values, while most experiments are performed at room temperature.

For the *ab initio* calculation of the SOECs, first one has to optimize lattice parameters and ionic positions. This optimization has been performed for all the crystal systems we have studied. The results for the equilibrium lattice parameters of the different materials are shown in Table 8 for all the used codes. The errors concerning the numerical differentiation have been minimized by using the procedure shown in Section 4. Obviously, the different codes (`exciting`, WIEN2k, and Quantum ESPRESSO)

**Table 8**

Optimized lattice parameters ( $a$ ,  $b$ , and  $c$ , in atomic units) and angles ( $\alpha$ ,  $\beta$ , and  $\gamma$ , in degrees) for representative materials.  $\mathcal{X}$ ,  $\mathcal{W}$ , and  $\mathcal{Q}$  denote calculations performed with the codes `exciting`, `WIEN2k`, and `Quantum ESPRESSO`, respectively. For elemental Ti, the labels (us) and (paw) indicate the use of ultra-soft pseudopotentials or the Projector-Augmented-Wave method, respectively. The quoted references refer to experimental values.

Material	Code	$a$	$b$	$c$	$\alpha$	$\beta$	$\gamma$
C	$\mathcal{X}$	6.747					
	$\mathcal{W}$	6.749					
	$\mathcal{Q}$	6.741					
	[34]	6.741					
Al	$\mathcal{W}$	7.636					
	$\mathcal{Q}$	7.669					
	[35]	7.653					
CsCl	$\mathcal{W}$	7.702					
	[36]	7.797					
Ti	$\mathcal{W}$	5.552		8.803			
	$\mathcal{Q}$ (paw)	5.555		8.791			
	$\mathcal{Q}$ (us)	5.412		8.554			
	[37]	5.575		8.844			
TiB <sub>2</sub>	$\mathcal{W}$	5.729		6.107			
	$\mathcal{Q}$	5.727		6.079			
	[38]	5.726		6.108			
Al <sub>2</sub> O <sub>3</sub>	$\mathcal{W}$	9.800			55.28		
	$\mathcal{Q}$	9.741			55.29		
	[39]	9.691			55.28		
CaMg(CO <sub>3</sub> ) <sub>2</sub>	$\mathcal{Q}$	11.439			47.24		
	[40]	11.363			47.12		
MgF <sub>2</sub>	$\mathcal{W}$	8.898		5.857			
	$\mathcal{Q}$	8.873		5.855			
	[41]	8.721		5.750			
CaMoO <sub>4</sub>	$\mathcal{W}$	10.003		21.931			
	$\mathcal{Q}$	10.061		21.881			
	[42]	9.868		21.590			
TiSi <sub>2</sub>	$\mathcal{W}$	9.072	15.654	16.200			
	$\mathcal{Q}$	9.048	15.624	16.204			
	[43]	9.071	15.628	16.157			
ZrO <sub>2</sub>	$\mathcal{W}$	10.128	9.812	9.931			99.63
	$\mathcal{Q}$	10.138	9.786	9.897			99.62
	[44]	10.048	9.733	9.849			99.23
TiSi <sub>2</sub>	$\mathcal{W}$	9.284	9.047	11.264	53.04	51.14	75.82

and different approaches (energy and stress) should achieve very similar results. If this is not the case, the failure should be attributed to the one or the other approximation which is implicit in the theoretical methods or in their implementation.

Below, results for the different types of crystal structures are discussed separately.

### 7.1. Cubic family

For cubic crystal structures, the second-order elastic tensor is fully determined by three independent elastic constants. We have chosen three examples representing different ranges of elastic moduli: diamond, Al, and CsCl, which are known as hard, medium, and soft material, respectively. Hard materials, like diamond, are characterized by very deep energy–strain and very steep stress–strain curves. This situation corresponds to relatively large values of SOECs. On the other hand, in soft materials like CsCl, the curves representing the energy/stress as a function of the strain are much flatter, which can cause larger errors in the resulting elastic properties. In fact, while a given accuracy in the evaluation of the total energy may lead to small errors for hard materials, the same accuracy may yield large errors for a soft material.

In Tables 9 and 10, the SOECs obtained with different approaches and codes are shown. As can be seen in Table 9, all the

**Table 9**

Elastic constants ( $c_{\alpha\beta}$ ) for single-crystal C with the cubic diamond structure. We also show results for the isotropic bulk ( $B$ ) and shear ( $G$ ) modulus for poly-crystalline samples obtained using both the Voigt and Reuss averaging procedure. (Note that for cubic structures  $B_V = B_R = B$ .) The Young's modulus ( $E$ ) and Poisson's ratio ( $\nu$ ) are estimated from Hill's approximation. All data except  $\nu$ , which is dimensionless, are given in GPa. The symbols  $\mathcal{W}$ ,  $\mathcal{X}$ , and  $\mathcal{Q}$  denote calculations performed with the codes `WIEN2k`, `exciting`, and `Quantum ESPRESSO`, respectively. The subscripts  $\mathcal{E}$  and  $\tau$  indicate the use of the energy and stress approach, respectively. Source: Experimental values for the elastic constants are taken from Ref. [45], the experimental elastic moduli are obtained from these values using Eqs. (11)–(18).

C	$\mathcal{W}_{\mathcal{E}}$	$\mathcal{X}_{\mathcal{E}}$	$\mathcal{Q}_{\mathcal{E}}$	$\mathcal{Q}_{\tau}$	[45]
$c_{11}$	1052.3	1055.9	1052.7	1053.0	1077.0
$c_{12}$	125.0	125.1	121.5	121.3	124.6
$c_{44}$	559.3	560.6	560.3	560.6	577.0
$B$	434.1	435.4	431.9	431.8	442.1
$G_V$	521.0	522.5	522.4	522.7	536.7
$G_R$	516.7	518.2	518.2	518.4	532.0
$E_H$	1113.1	1116.3	1113.7	1114.0	1142.6
$\nu_H$	0.07	0.07	0.07	0.07	0.07

**Table 10**

Same as Table 9 for Al (left) and CsCl (right) in the cubic structure. Source: Data from Refs. [45,46] are experimental values.

	Al				CsCl	
	$\mathcal{W}_{\mathcal{E}}$	$\mathcal{Q}_{\mathcal{E}}$	$\mathcal{Q}_{\tau}$	[45]	$\mathcal{W}_{\mathcal{E}}$	[46]
$c_{11}$	112.1	109.3	109.0	108.0	36.9	36.4
$c_{12}$	60.3	57.5	57.7	62.0	8.4	8.8
$c_{44}$	32.8	30.1	34.6	28.3	8.4	8.0
$B$	77.6	74.8	74.8	77.3	17.9	18.0
$G_V$	30.1	28.4	31.0	26.2	10.8	10.3
$G_R$	29.7	28.3	30.4	25.9	10.8	9.6
$E_H$	79.4	75.5	81.1	70.2	26.2	25.2
$\nu_H$	0.33	0.33	0.32	0.35	0.26	0.27

theoretical results for diamond are very similar and very close to calculated [11] and experimental data [45]. In Ref. [11] the elastic constants have been computed from stress using the VASP code. The largest deviation, between our results and experimental data, is found for the values of  $c_{11}$  and  $c_{44}$  which appear smaller than in experiment. The tendency of GGA to slightly overestimate the bonding strength corresponds to an underestimation of the crystal's stiffness. For Al and CsCl, the agreement of all the values with their experimental counterparts (see Table 10) is also very good.

### 7.2. Hexagonal family

Among the two members of the hexagonal family (see Table 1), we first discuss the primitive hexagonal structures. There are five independent elastic constants. As representative for this crystal system, the elemental metal Ti and the metal-like ceramic TiB<sub>2</sub> have been chosen. According to the results presented in Tables 11 and 12, elastic constants for TiB<sub>2</sub> obtained with different methods and codes are very similar, while for Ti large deviations are observed among theoretical results obtained with different pseudopotentials. SOECs calculated using the PAW method [47], are very close to the ones obtained by the WIEN2k code. In contrast, the results based on ultra-soft (us) potentials [48] are significantly different. These deviations indicate a failure of this kind of pseudo-potential approximation for describing the metallic interaction in hexagonal titanium.

In Tables 13 and 14, we list the calculated elastic constants for materials belonging to the trigonal family. In trigonal lattices, there are either six or seven independent elastic constants, and the two cases are distinguishable on the basis of the SGN. We have chosen Al<sub>2</sub>O<sub>3</sub> and CaMg(CO<sub>3</sub>)<sub>2</sub> as examples for the Laue groups  $R_1$  and  $R_{11}$ , respectively. The calculation of the SOECs for trigonal

**Table 11**

Same as Table 9 for  $\text{TiB}_2$  in the primitive hexagonal structure.  
Source: Data from Ref. [49] are experimental values.

$\text{TiB}_2$	$\mathcal{W}_\varepsilon$	$\mathcal{Q}_\varepsilon$	$\mathcal{Q}_\tau$	[49]
$c_{11}$	652	654	652	660
$c_{12}$	69	71	69	48
$c_{13}$	103	100	98	93
$c_{33}$	448	459	463	432
$c_{44}$	258	260	259	260
$B_V$	256	256	256	247
$B_R$	250	251	251	240
$G_V$	260	262	262	266
$G_R$	254	257	257	258
$E_H$	576	581	581	579
$\nu_H$	0.12	0.12	0.12	0.10

**Table 12**

Same as Table 9 for Ti in the primitive hexagonal structure. The labels (us) and (paw) indicate the use of ultra-soft pseudo-potentials and the PAW method, respectively.  
Source: Data from Ref. [50] are experimental values.

Ti	$\mathcal{W}_\varepsilon$	$\mathcal{Q}_\varepsilon^{(\text{paw})}$	$\mathcal{Q}_\varepsilon^{(\text{us})}$	[50]
$c_{11}$	179	174	190	160
$c_{12}$	85	85	99	90
$c_{13}$	74	77	91	66
$c_{33}$	187	181	213	181
$c_{44}$	44	44	39	46
$B_V$	112	112	128	105
$B_R$	112	112	128	105
$G_V$	48	46	45	44
$G_R$	48	46	44	42
$E_H$	125	120	120	114
$\nu_H$	0.31	0.32	0.34	0.32

crystals deserves special attention. First, there is an intrinsic difference between trigonal crystal structures of type  $P$  and  $R$  (see Table 1). In contrast to the structures with  $R$  centering, the primitive  $P$  structures are treated on the same footing as the primitive hexagonal ones. Second, the default choice of the reference Cartesian coordinate frame used for these crystals is not the same for all DFT codes. As a consequence, for the trigonal family, the calculated second-order elastic matrix can be different as well, as demonstrated below. The different choices of the default Cartesian reference frame defined in ELAStic for the DFT codes considered in this work are presented in the Appendix (Table A.20).

According to the literature concerning the SOECs in trigonal materials with  $R$  centering type, the sign of  $c_{14}$  and  $c_{15}$  is an open issue. Different signs of  $c_{14}$  of  $\text{Al}_2\text{O}_3$  are found in experimental [51–54] as well as theoretical work [55–58]. These discrepancies may be related to the ambiguity in the choice of the Cartesian coordinate frame for the trigonal structure of type  $R$ . In the literature, this structure is often referred to as *rhombohedral*, and this denomination will be adopted in the following. Systems with rhombohedral symmetry can be described using a supercell with hexagonal symmetry. The setting of the hexagonal primitive cell with respect to the rhombohedral unit cell is not unique, allowing for different choices of the Cartesian reference frame. An additional complication appears, as in different DFT codes the Cartesian frames are defined differently (see Table A.20). In order to sketch the situation, we show in Fig. 6 two different choices for the hexagonal unit cell for the rhombohedral cell of  $\text{Al}_2\text{O}_3$  together with the rhombohedral primitive vectors projected onto the  $xy$  plane. The two Cartesian reference frames are labeled by “+” and “–”, which correspond to the sign of  $c_{14}$  in our calculated examples. As can be seen in Tables 13 and 14, our calculated values of  $c_{14}$  for  $\text{Al}_2\text{O}_3$  and  $\text{CaMg}(\text{CO}_3)_2$  are negative, which is consistent with the choice of the “–” Cartesian coordinate system in the ELAStic code.

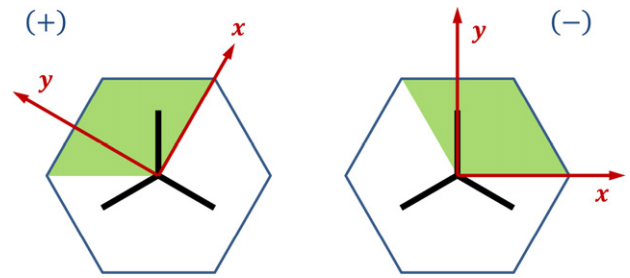


**Fig. 6.** Two possible choices for Cartesian coordinates in the trigonal  $R$  (rhombohedral) structure. For the coordinate system in the right (left) panel, negative (positive) values are obtained for  $c_{14}$  for  $\text{Al}_2\text{O}_3$ . Black bold lines indicate the projection of the primitive rhombohedral lattice vectors onto the  $xy$  plane. The shaded (green) areas correspond to the hexagonal primitive cells. (For interpretation of the references to colour in this figure legend, the reader is referred to the web version of this article.)

**Table 13**

Same as Table 9 for  $\text{Al}_2\text{O}_3$  in the trigonal  $R$  structure.  
Source: Data from Ref. [50] are experimental values.

$\text{Al}_2\text{O}_3$	$\mathcal{W}_\varepsilon$	$\mathcal{Q}_\varepsilon$	$\mathcal{Q}_\tau$	[50]
$c_{11}$	453.4	463.8	460.9	497.4
$c_{12}$	151.2	148.5	148.7	164.0
$c_{13}$	108.0	107.9	107.8	112.2
$c_{14}$	–20.5	–20.3	–20.4	–23.6
$c_{33}$	452.0	469.9	466.4	499.1
$c_{44}$	132.2	139.0	137.6	147.4
$B_V$	232.6	236.2	235.2	252.3
$B_R$	232.2	236.0	234.9	251.8
$G_V$	149.2	156.0	154.5	166.0
$G_R$	144.7	151.7	150.2	160.6
$E_H$	364.1	379.3	375.8	403.0
$\nu_H$	0.24	0.23	0.23	0.23

**Table 14**

Same as Table 9 for  $\text{CaMg}(\text{CO}_3)_2$  (dolomite) in the trigonal  $R_{II}$  structure.  
Source: Data from Ref. [59] are experimental values.

$\text{CaMg}(\text{CO}_3)_2$	$\mathcal{Q}_\varepsilon$	$\mathcal{Q}_\tau$	[59]
$c_{11}$	194.3	194.5	205.0
$c_{12}$	66.5	66.7	71.0
$c_{13}$	56.8	56.4	57.4
$c_{14}$	–17.5	–17.7	–19.5
$c_{15}$	11.5	11.1	13.7
$c_{33}$	108.5	107.4	113.0
$c_{44}$	38.8	38.6	39.8
$B_V$	95.3	95.0	99.4
$B_R$	87.2	86.6	90.3
$G_V$	49.4	49.4	51.8
$G_R$	39.4	39.3	39.7
$E_H$	114.7	114.4	118.2
$\nu_H$	0.29	0.29	0.29

### 7.3. Tetragonal and orthorhombic families

Our results for crystals with tetragonal  $T_I$  and  $T_{II}$  as well as orthorhombic symmetry are summarized in Tables 15–17, respectively. In tetragonal systems, there are either six ( $T_I$  class) or seven ( $T_{II}$ ) independent elastic constants. We have studied  $\text{MgF}_2$  and  $\text{CaMoO}_4$  as examples for the  $T_I$  and  $T_{II}$  lattice types, respectively. All calculated results are in reasonable agreement with experiment. The stress and energy approach, as well as the use of WIEN2k and Quantum ESPRESSO, lead to similar elastic constants, except for  $c_{12}$  for  $\text{CaMoO}_4$  obtained with the WIEN2k code.

The SOECs for the orthorhombic system  $\text{TiSi}_2$  are listed in Table 17. In this case, there are nine independent elastic constants. The comparison between the values obtained by pseudo-potential calculations with the full-potential and experimental results shows large deviations for some elastic constants, e.g.,  $c_{13}$ ,  $c_{22}$ ,  $c_{33}$ , and  $c_{66}$ . Such discrepancies have also been reported

**Table 15**

Same as Table 9 for  $\text{MgF}_2$  in the tetragonal  $T_1$  structure.  
Source: Data from Ref. [60] are experimental values.

$\text{MgF}_2$	$W_\varepsilon$	$Q_\varepsilon$	$Q_\tau$	[60]
$c_{11}$	130.0	127.0	126.5	123.7
$c_{12}$	78.2	80.1	79.8	73.2
$c_{13}$	54.7	57.3	57.6	53.6
$c_{33}$	185.0	187.7	187.3	177.0
$c_{44}$	50.5	50.8	50.7	55.2
$c_{66}$	83.0	87.2	87.2	97.8
$B_V$	91.1	92.3	92.2	87.2
$B_R$	90.5	91.4	91.3	86.4
$G_V$	54.0	54.2	54.0	57.9
$G_R$	46.7	45.2	45.0	48.1
$E_H$	127.4	126.3	126.0	132.1
$\nu_H$	0.27	0.27	0.27	0.25

**Table 16**

Same as Table 9 for  $\text{CaMoO}_4$  in the tetragonal  $T_{II}$  structure.  
Source: Data from Ref. [61] are experimental values.

$\text{CaMoO}_4$	$W_\varepsilon$	$Q_\varepsilon$	$Q_\tau$	[61]
$c_{11}$	123.4	126.9	125.9	144.7
$c_{12}$	43.9	58.0	57.5	66.4
$c_{13}$	48.7	46.6	46.0	46.6
$c_{16}$	8.1	10.2	10.1	13.4
$c_{33}$	109.3	110.0	109.3	126.5
$c_{44}$	31.5	29.0	28.7	36.9
$c_{66}$	37.4	34.2	34.2	45.1
$B_V$	71.0	74.0	73.4	81.7
$B_R$	70.9	73.2	72.6	80.5
$G_V$	34.4	32.6	32.4	40.9
$G_R$	33.5	31.1	30.9	38.7
$E_H$	87.8	83.5	83.0	102.6
$\nu_H$	0.29	0.31	0.31	0.29

**Table 17**

Same as Table 9 for  $\text{TiSi}_2$  in the orthorhombic structure. For titanium, an ultra-soft pseudo-potential has been used for calculations performed with Quantum ESPRESSO.

Source: Data from Ref. [62] are experimental values.

$\text{TiSi}_2$	$W_\varepsilon$	$Q_\varepsilon$	$Q_\tau$	[62]
$c_{11}$	312.5	297.9	306.4	320.4
$c_{12}$	27.9	18.5	24.8	29.3
$c_{13}$	83.8	123.3	112.3	86.0
$c_{22}$	306.3	212.2	204.6	317.5
$c_{23}$	21.1	31.2	31.5	38.4
$c_{33}$	406.4	481.9	495.8	413.2
$c_{44}$	73.1	73.6	73.2	75.8
$c_{55}$	106.4	108.7	100.0	112.5
$c_{66}$	117.3	97.5	106.0	117.5
$B_V$	143.4	148.7	149.4	150.9
$B_R$	139.4	124.0	124.1	146.8
$G_V$	118.8	110.5	111.7	120.9
$G_R$	110.0	101.2	101.6	112.9
$E_H$	270.3	252.3	253.9	278.1
$\nu_H$	0.180	0.190	0.190	0.188

in Ref. [11]. Like before, we assign them to the pseudo-potential approximation.

#### 7.4. Monoclinic and triclinic families

The monoclinic structure is characterized by thirteen independent elastic constants. Due to the large number of SOECs and the low symmetry, calculations for this structure family are computationally more demanding than for the previous ones. We have chosen  $\text{ZrO}_2$  as representative material.

Theoretical data for monoclinic zirconia are listed in Table 18. The choice of Cartesian reference frame for monoclinic structures in the codes Quantum ESPRESSO and WIEN2k is different, as shown in Appendix. Therefore, in order to compare results of

**Table 18**

Same as Table 9 for  $\text{ZrO}_2$  (zirconia) in the monoclinic structure.

Source: Data from Ref. [9] are obtained using the CASTEP code and the stress approach whereas Ref. [63] is the experiment.

$\text{ZrO}_2$	$W_\varepsilon$	$Q_\varepsilon$	$Q_\tau$	[9]	[63]
$c_{11}$	356	334	333	341	361
$c_{12}$	161	151	157	158	142
$c_{13}$	76	82	85	88	55
$c_{15}$	32	32	28	29	-21
$c_{22}$	361	356	363	349	408
$c_{23}$	120	142	154	156	196
$c_{25}$	-3	-2	-6	-4	31
$c_{33}$	217	251	258	274	258
$c_{35}$	2	7	3	2	-18
$c_{44}$	80	81	80	80	100
$c_{46}$	-16	-15	-15	-14	-23
$c_{55}$	69	71	71	73	81
$c_{66}$	113	115	115	116	126
$B_V$	183	188	194	196	201
$B_R$	163	174	181	187	175
$G_V$	91	91	90	91	91
$G_R$	83	84	83	84	84
$E_H$	223	226	225	229	226
$\nu_H$	0.28	0.29	0.30	0.30	0.29

different codes, we have transformed all the elastic constants to the Cartesian coordinate system used in experiment [63] applying Eq. (19). Deviations between theory and experiment may be related to temperature effects.

Triclinic structures exhibit the lowest symmetry, where all the 21 Voigt components of the elastic tensor are independent. Moreover, triclinic materials typically, have more than ten atoms in the unit cell. Hence, in this case the calculations are very demanding. In order to make calculations feasible at reasonable computational cost, we have chosen the primitive orthorhombic cell of  $\text{TiSi}_2$  as an example, but treating it without considering symmetry. Instead of comparing with experiment, we have made a comparison between the elastic constants calculated directly for the triclinic primitive unit cell and those obtained from the transformation of the previous results for the orthorhombic unit cell. The comparison is shown in Table 19.

## 8. Summary and discussion

We have introduced *ElaStic*, a tool for calculating second-order elastic constants using two alternative approaches, based on the calculation of the total energy and stress, respectively. The two approaches provide equivalent results, but have some intrinsic differences.

The stress approach allows to use a much smaller set of deformations, thus reducing the computational effort. Furthermore, only first-order derivatives have to be calculated, which improve the accuracy of numerical differentiation. However, the symmetry of the distorted structures in this case is lowered to monoclinic or triclinic, thereby increasing CPU time and memory consumption. In order to achieve the same accuracy by directly computing the stress tensor rather than through total-energy calculations, often computational parameters (e.g., kinetic-energy cutoff,  $\mathbf{k}$ -point sampling, etc.) have to be readjusted, which increases the computational costs. In addition, this direct calculation of the stress tensor is not available in every considered code.

On the other hand, a larger number of distortion types must be considered for the energy approach, which also requires the numerical calculation of second-order derivatives. Deformation types, however, can be selected such to preserve the symmetry of the reference system as much as possible. For more symmetric crystal structures, e.g. cubic or hexagonal, both approaches are equally suitable, but for less symmetric crystal structures like monoclinic or triclinic systems, the stress approach is more efficient.

**Table 19**

Elastic constants (in GPa) for single crystal TiSi<sub>2</sub> in the triclinic structure calculated using the WIEN2k code. Values of the first row are the results from direct calculations in the triclinic unit cell; the second row is obtained by transforming the results from the centrosymmetric orthorhombic unit cell (lattice class O) to the triclinic structure (N) using Eq. (19).

	$c_{11}$	$c_{12}$	$c_{13}$	$c_{14}$	$c_{15}$	$c_{16}$	$c_{22}$	$c_{23}$	$c_{24}$	$c_{25}$	$c_{26}$	$c_{33}$	$c_{34}$	$c_{35}$
Direct calculations	354.5	42.2	88.6	−31.4	27.4	−14.4	284.1	48.9	17.2	7.5	14.8	287.3	−17.0	−4.6
Transform from O to N	361.1	39.8	89.6	−33.8	30.4	−15.3	285.0	48.8	15.4	5.9	14.0	288.4	−17.7	−3.1
	$c_{36}$	$c_{44}$	$c_{45}$	$c_{46}$	$c_{55}$	$c_{56}$	$c_{66}$	$B_V$	$B_R$	$G_V$	$G_R$	$E_H$	$\nu_H$	
Direct calculations	−14.0	128.9	−4.0	−8.8	119.3	−17.5	92.6	142.8	139.3	117.9	109.6	269.0	0.18	
Transform from O to N	−15.4	129.3	−8.2	−8.3	120.0	−18.4	92.9	143.4	139.4	118.8	110.0	279.4	0.18	

**Table A.20**

Lattice type (in the Laue group notation of Table 1), centering type(s), and Cartesian components of conventional lattice vectors ( $\mathbf{a}$ ,  $\mathbf{b}$ , and  $\mathbf{c}$ ) as defined in ElaStic when using the codes exciting ( $\mathcal{X}$ ), WIEN2k ( $\mathcal{W}$ ), and Quantum ESPRESSO ( $\mathcal{Q}$ ).  $\alpha$ ,  $\beta$ , and  $\gamma$  are the angles  $\widehat{bc}$ ,  $\widehat{ac}$ , and  $\widehat{ab}$ , respectively. The symbol  $\xi_\vartheta$  ( $\kappa_\vartheta$ ) represents the sine (cosine) of the angle  $\vartheta$ .  $M^{(b)}$  and  $M^{(c)}$  indicate the monoclinic crystal system with the  $b$  and  $c$  axis as unique axis, respectively.

Laue group	Centering type(s)	$\mathbf{a}$	$\mathbf{b}$	$\mathbf{c}$	$\mathcal{X}$	$\mathcal{W}$	$\mathcal{Q}$
$C_{1,II}$	$P, F, I$	$(a, 0, 0)$	$(0, a, 0)$	$(0, 0, a)$	✓	✓	✓
$H_{1,II}$	$P$	$(a, 0, 0)$	$(-\frac{1}{2}a, \frac{\sqrt{3}}{2}a, 0)$	$(0, 0, c)$	✓	✓	✓
$R_{1,II}$	$P$	$(a, 0, 0)$	$(-\frac{1}{2}a, \frac{\sqrt{3}}{2}a, 0)$	$(0, 0, c)$	✓	✓	✓
$T_{1,II}$	$R$	$(\tilde{a}, -\frac{1}{\sqrt{3}}\tilde{a}, h)$	$(0, \frac{2}{\sqrt{3}}\tilde{a}, h)$	$(-\tilde{a}, -\frac{1}{\sqrt{3}}\tilde{a}, h)$	✓	✓	✓
$T_{1,II}$	$P, I$	$(a, 0, 0)$	$(0, a, 0)$	$(0, 0, c)$	✓	✓	✓
O	$P, C, F, I$	$(a, 0, 0)$	$(0, b, 0)$	$(0, 0, c)$	✓	✓	✓
$M^{(b)}$	$P, C$	$(a, 0, 0)$	$(0, b, 0)$	$(c \kappa_\beta, 0, c \xi_\beta)$	×	×	✓
$M^{(c)}$	$P, C$	$(a, 0, 0)$	$(b \kappa_\gamma, b \xi_\gamma, 0)$	$(0, 0, c)$	✓	×	✓
		$(a \xi_\gamma, a \kappa_\gamma, 0)$	$(0, b, 0)$	$(0, 0, c)$	✓	✓	×
N	$P$	$(a, 0, 0)$	$(b \kappa_\gamma, b \xi_\gamma, 0)$	$(c \kappa_\beta, \tilde{c}, w)$	✓	✓	✓

$$\tilde{a} = a \xi_{\alpha/2}$$

$$h = a \sqrt{1 - \frac{4}{3} \xi_{\alpha/2}^2}$$

$$\tilde{c} = c \xi_\gamma^{-1} (\kappa_\alpha - \kappa_\beta \kappa_\gamma)$$

$$w = c \xi_\gamma^{-1} \sqrt{1 + 2\kappa_\alpha \kappa_\beta \kappa_\gamma - \kappa_\alpha^2 - \kappa_\beta^2 - \kappa_\gamma^2}$$

In order to demonstrate the ability and trustability of ElaStic, we have presented SOECs for prototypical example materials of all crystal families. The results produced with different codes based on total-energy calculations, are in good agreement with each other. Comparing results from the total-energy and the stress approach calculated with Quantum ESPRESSO are also consistent, emphasizing that both procedures are suitable and comparable for the calculations of elastic constants.

Finally, we want to emphasize that it is crucial to precisely determine numerical derivatives of the energy (or stress) of a crystal with respect to the Lagrangian strain in order to obtain reliable results for elastic constants. To this extent, we have developed a numerical method which allows to do so in an automatized manner.

ElaStic is freely available and can be downloaded from <http://exciting-code.org>.

## Acknowledgments

This work was carried out in the framework of the Competence Centre for Excellent Technologies (COMET) on Integrated Research in Materials, Processing and Product Engineering (MPPE), and Sim-Net Styria. Financial support by the Austrian Federal Government and the Styrian Provincial Government is acknowledged. We thank B.Z. Yanchitsky for allowing us the use of the SGROUP code, and Lorenz Romaner for fruitful discussions.

## Appendix

In general, crystal properties that are expressed by a tensor or a matrix, like elastic properties, depend on the choice of both the crystal axes and the Cartesian reference frame. That means that

the value of the elastic constants may change from one choice to another. Therefore, the comparison of calculated elastic constants with results of other calculations or experimental data is only possible provided the chosen crystal axes and reference frame are identical. For the sake of clarity, we present the definition of the *standard reference* (STD) for the crystal axes and the Cartesian reference frame which are used by ElaStic when dealing with different DFT computer packages. In addition, we show the independent components of the second-order elastic tensor for all the crystal types following from the STD. In the determination of the STD, ElaStic follows the *Standards on Piezoelectric Crystals* (1949), as recommended in Ref. [64].

For high-symmetry crystal systems, such as the cubic one, this choice of reference is obvious. However, the situation is different for lower-symmetry structures. Due to this fact, different software packages may define Cartesian coordinate axes in different ways which are not necessarily the same as the STD. For instance, the definition of the Cartesian coordinate system for the hexagonal crystal family in WIEN2k is different from the standard one. Furthermore, for some crystals, there exists more than one choice of reference axes which are compatible with the standard, which is, e.g., the case for the monoclinic crystal system. For this system, the lattice vector parallel to the two-fold axis, which is called unique axis, could be either  $\mathbf{b}$  or  $\mathbf{c}$ . We denote these different choices as  $M^{(b)}$  and  $M^{(c)}$ , respectively. The non-zero SOECs are different for these two cases (see Table A.21).

The Cartesian components of conventional (primitive) lattice vectors ( $\mathbf{a}$ ,  $\mathbf{b}$ , and  $\mathbf{c}$ ) as defined in ElaStic when applied in combination with different codes are shown in Table A.20. In the subsequent Table A.21, we display the independent SOECs corresponding to each lattice type for the STD.

**Table A.21**

Symmetry properties of the matrix of SOECs for each Laue group class. Elastic constants are referred to Cartesian axes according to Table A.20.

Laue group											
$C_{I,II}$	$H_{I,II}$	$R_I$	$R_{II}$	$T_I$	$T_{II}$	O	$M^{(b)}$	$M^{(c)}$	N		
$C_{11}$	$C_{11}$	$C_{11}$	$C_{11}$	$C_{11}$	$C_{11}$	$C_{11}$	$C_{11}$	$C_{11}$	$C_{11}$	$C_{11}$	$C_{11}$
$C_{12}$	$C_{12}$	$C_{12}$	$C_{12}$	$C_{12}$	$C_{12}$	$C_{12}$	$C_{12}$	$C_{12}$	$C_{12}$	$C_{12}$	$C_{12}$
$C_{13}$	$C_{13}$	$C_{13}$	$C_{13}$	$C_{13}$	$C_{13}$	$C_{13}$	$C_{13}$	$C_{13}$	$C_{13}$	$C_{13}$	$C_{13}$
0	0	$C_{14}$	$C_{14}$	0	0	0	0	0	0	$C_{14}$	$C_{14}$
0	0	0	$C_{15}$	0	0	0	$C_{15}$	0	0	$C_{15}$	$C_{15}$
0	0	0	0	0	$C_{16}$	0	0	0	$C_{16}$	$C_{16}$	$C_{16}$
$C_{11}$	$C_{11}$	$C_{11}$	$C_{11}$	$C_{11}$	$C_{11}$	$C_{22}$	$C_{22}$	$C_{22}$	$C_{22}$	$C_{22}$	$C_{22}$
$C_{12}$	$C_{13}$	$C_{13}$	$C_{13}$	$C_{13}$	$C_{13}$	$C_{23}$	$C_{23}$	$C_{23}$	$C_{23}$	$C_{23}$	$C_{23}$
0	0	$-C_{14}$	$-C_{14}$	0	0	0	0	0	0	$C_{24}$	$C_{24}$
0	0	0	$-C_{15}$	0	0	0	$C_{25}$	0	0	$C_{25}$	$C_{25}$
0	0	0	0	0	$-C_{16}$	0	0	0	$C_{26}$	$C_{26}$	$C_{26}$
$C_{11}$	$C_{33}$	$C_{33}$	$C_{33}$	$C_{33}$	$C_{33}$	$C_{33}$	$C_{33}$	$C_{33}$	$C_{33}$	$C_{33}$	$C_{33}$
0	0	0	0	0	0	0	0	0	0	$C_{34}$	$C_{34}$
0	0	0	0	0	0	0	$C_{35}$	0	0	$C_{35}$	$C_{35}$
0	0	0	0	0	0	0	0	$C_{36}$	0	$C_{36}$	$C_{36}$
$C_{44}$	$C_{44}$	$C_{44}$	$C_{44}$	$C_{44}$	$C_{44}$	$C_{44}$	$C_{44}$	$C_{44}$	$C_{44}$	$C_{44}$	$C_{44}$
0	0	0	0	0	0	0	0	0	0	$C_{45}$	$C_{45}$
0	0	0	$-C_{15}$	0	0	0	$C_{46}$	0	0	$C_{46}$	$C_{46}$
$C_{44}$	$C_{44}$	$C_{44}$	$C_{44}$	$C_{44}$	$C_{44}$	$C_{55}$	$C_{55}$	$C_{55}$	$C_{55}$	$C_{55}$	$C_{55}$
0	0	$C_{14}$	$C_{14}$	0	0	0	0	0	0	$C_{56}$	$C_{56}$
$C_{44}$	$\frac{1}{2}(C_{11} - C_{12})$	$\frac{1}{2}(C_{11} - C_{12})$	$\frac{1}{2}(C_{11} - C_{12})$	$C_{66}$	$C_{66}$	$C_{66}$	$C_{66}$	$C_{66}$	$C_{66}$	$C_{66}$	$C_{66}$

Sometimes it is useful to transform the second-order elastic tensor to a different choice than the STD for the Cartesian frame. This can be accomplished with the help of Eq. (19), from the initial reference axes to the final coordinate system by applying the proper transformation matrix. In the following, we present some of the matrices that may be needed to transform the elastic constants.

- To transform the hexagonal crystal family (hexagonal and trigonal crystal systems) from the STD, which is used by ELAStic, to the coordinate system applied by WIEN2k, one has to use the following transformation matrix

$$T_H^{STD \rightarrow w} = \begin{pmatrix} -\frac{\sqrt{3}}{2} & \frac{1}{2} & 0 \\ \frac{1}{2} & \frac{\sqrt{3}}{2} & 0 \\ 0 & 0 & 1 \end{pmatrix}. \quad (A.1)$$

- As can be seen in Table A.20, there are two types of settings for monoclinic crystals in Quantum ESPRESSO. The elastic constants can be transformed from the  $M^{(b)}$  to the  $M^{(c)}$  representation by using the transformation matrix

$$T_M^{\mathcal{Q}_b \rightarrow \mathcal{Q}_c} = \begin{pmatrix} 1 & 0 & 0 \\ 0 & 0 & -1 \\ 0 & 1 & 0 \end{pmatrix}. \quad (A.2)$$

- The monoclinic settings of  $M^{(c)}$  in Quantum ESPRESSO and WIEN2k are different. The SOECs are comparable if the following matrix is applied to transform the calculated result of Quantum ESPRESSO to WIEN2k,

$$T_M^{\mathcal{Q}_c \rightarrow w_c} = \begin{pmatrix} -\sin(\gamma) & \cos(\gamma) & 0 \\ -\cos(\gamma) & \sin(\gamma) & 0 \\ 0 & 0 & 1 \end{pmatrix}. \quad (A.3)$$

## References

- [1] C.-M. Li, Q.-M. Hu, R. Yang, B. Johansson, L. Vitos, First-principles study of the elastic properties of In-Tl random alloys, Phys. Rev. B 82 (9) (2010) 094201.
- [2] G.V. Sin'ko, Ab initio calculations of the second-order elastic constants of crystals under arbitrary isotropic pressure, Phys. Rev. B 77 (10) (2008) 104118.
- [3] S. Shang, Y. Wang, Z.-K. Liu, First-principles elastic constants of  $\alpha$ - and  $\theta$ -Al<sub>2</sub>O<sub>3</sub>, Appl. Phys. Lett. 90 (2007) 101909.
- [4] K.B. Panda, K.S.R. Chandran, Determination of elastic constants of titanium diboride (TiB<sub>2</sub>) from first principles using flapw implementation of the density functional theory, Comput. Mater. Sci. 35 (2) (2006) 134–150.
- [5] C. Bercegeay, S. Bernard, First-principles equations of state and elastic properties of seven metals, Phys. Rev. B 72 (21) (2005) 214101.
- [6] G. Steinle-Neumann, L. Stixrude, R.E. Cohen, First-principles elastic constants for the hcp transition metals Fe, Co, and Re at high pressure, Phys. Rev. B 60 (2) (1999) 791–799.
- [7] P. Ravindran, L. Fast, P.A. Korzhavyi, B. Johansson, Density functional theory for calculation of elastic properties of orthorhombic crystals: application to TiSi<sub>2</sub>, J. Appl. Phys. 84 (9) (1998) 4891.
- [8] H. Yao, L. Ouyang, W.-Y. Ching, Ab initio calculation of elastic constants of ceramic crystals, J. Am. Ceram. Soc. 90 (10) (2007) 3193–3204.
- [9] M. Iuga, G. Steinle-Neumann, J. Meinhart, Ab-initio simulation of elastic constants for some ceramic materials, Eur. Phys. J. B 58 (2) (2007) 127–133.
- [10] W.F. Perger, J. Criswell, B. Civalleri, R. Dovesi, Ab-initio calculation of elastic constants of crystalline systems with the crystal code, Comput. Phys. Comm. 180 (10) (2009) 1753–1759.
- [11] R. Yu, J. Zhu, H.Q. Ye, Calculations of single-crystal elastic constants made simple, Comput. Phys. Comm. 181 (3) (2010) 671–675.
- [12] P. Hohenberg, W. Kohn, Inhomogeneous electron gas, Phys. Rev. 136 (3B) (1964) B864–B871.
- [13] W. Kohn, L.J. Sham, Inhomogeneous electron gas, Phys. Rev. 140 (1965) A1133.
- [14] D.C. Langreth, B.I. Lundqvist, S.D. Chakarova-Käck, V.R. Cooper, M. Dion, P. Hyldgaard, A. Kelkkanen, J. Kleis, L. Kong, S. Li, P.G. Moses, E. Murray, A. Puzder, H. Rydberg, E. Schröder, T. Thonhauser, A density functional for sparse matter, J. Phys.: Condens. Matter 21 (2009) 084203.
- [15] D. Nabok, P. Puschnig, C. Ambrosch-Draxl, NoloCo: an efficient implementation of van der Waals density functionals based on a Monte-Carlo integration technique, Comput. Phys. Comm. 128 (2011) 1657–1662.
- [16] D. Wallace, Thermodynamics of Crystals, in: Dover Books on Physics, Dover Publications, 1998.
- [17] O.H. Nielsen, R.M. Martin, First-principles calculation of stress, Phys. Rev. Lett. 50 (9) (1983) 697–700.
- [18] O.H. Nielsen, R.M. Martin, Stresses in semiconductors: Ab initio calculations on Si, Ge, and GaAs, Phys. Rev. B 32 (1985) 3792–3805.
- [19] B.Z. Yanchitsky, A.N. Timoshevskii, Determination of the space group and unit cell for a periodic solid, Comput. Phys. Comm. 139 (2001) 235–242.
- [20] W. Voigt, Lehrbuch der Kristallphysik, B.G. Teubner, 1928.
- [21] A. Reuss, Z. Angew. Berchung der Fließgrenze von Mischkristallen auf Grund der Plastizitätsbedingung für Einkristalle, Math. Mech. 9 (1929) 49–58.
- [22] R. Hill, The elastic behaviour of a crystalline aggregate, Proc. Phys. Soc. A 65 (1952) 349.
- [23] R. Hill, Elastic properties of reinforced solids: some theoretical principles, J. Mech. Phys. Solids 11 (1963) 357.
- [24] S. Geisser, Predictive Inference: An Introduction, Chapman and Hall, New York, 1993.
- [25] P.A. Devijver, J. Kittler, Pattern Recognition: A Statistical Approach, Prentice/Hall International, 1982.
- [26] A. van de Walle, G. Ceder, Automating first-principles phase diagram calculations, J. Phase Equilib. 23 (2002) 348–359.
- [27] F. Birch, Finite elastic strain of cubic crystals, Phys. Rev. 71 (11) (1947) 809–824.

- [28] M.J. Mehl, Occupation-number broadening schemes: choice of temperature, *Phys. Rev. B* 61 (3) (2000) 1654–1657.
- [29] J.P. Perdew, K. Burke, Y. Wang, Generalized gradient approximation for the exchange–correlation hole of a many-electron system, *Phys. Rev. B* 54 (23) (1996) 16533–16539.
- [30] J.P. Perdew, A. Ruzsinszky, G.I. Csonka, O.A. Vydrov, G.E. Scuseria, L.A. Constantin, X. Zhou, K. Burke, Restoring the density-gradient expansion for exchange in solids and surfaces, *Phys. Rev. Lett.* 100 (2008) 136406.
- [31] P.E. Blöchl, O. Jepsen, O.K. Andersen, Improved tetrahedron method for Brillouin-zone integrations, *Phys. Rev. B* 49 (1994) 16223–16233.
- [32] H.J. Monkhorst, J.D. Pack, Special points for Brillouin-zone integrations, *Phys. Rev. B* 13 (12) (1976) 5188.
- [33] M. Methfessel, A.T. Paxton, High-precision sampling for Brillouin-zone integration in metals, *Phys. Rev. B* 40 (6) (1989) 3616.
- [34] T. Hom, W. Kiszczek, B. Post, Accurate lattice constants from multiple reflection measurements. II. Lattice constants of germanium silicon, and diamond, *J. Appl. Crystallogr.* 8 (4) (1975) 457–458.
- [35] G. Chiarotti, 1.6 Crystal structures and bulk lattice parameters of materials quoted in the volume, in: Landolt–Börnstein–Group III Condensed Matter Numerical Data and Functional Relationships in Science and Technology, vol. 24c, Springer-Verlag, 1995.
- [36] V. Ganesan, K. Girirajan, Lattice parameter and thermal expansion of CsCl and CsBr by x-ray powder diffraction. I. Thermal expansion of CsCl from room temperature to 90K, *Pramana J. Phys.* 27 (1986) 472.
- [37] J. Donohue, The Structures of the Elements, A Wiley-Interscience Publication, Wiley, 1974.
- [38] L.N. Kugai, *Inorg. Chem.* 8 (1972) 669.
- [39] W.E. Lee, K.P.D. Lagerlof, Structural and electron diffraction data for sapphire ( $\alpha$ -Al<sub>2</sub>O<sub>3</sub>), *J. Electron Microsc. Tech.* 2 (1985) 247–258.
- [40] R.J. Reeder, S.A. Markgraf, High-temperature crystal chemistry of dolomite, *Am. Mineral.* 71 (1986) 795–804.
- [41] G. Vidal-Valat, J.P. Vidal, C.M.E. Zeyen, K. KurkiSuonio, *Acta Crystallogr. Sect. B* 35 (1979) 1584.
- [42] R.M. Hazen, L.W. Finger, J.W.E. Mariathasan, *J. Phys. Chem. Solids* 46 (1985) 253.
- [43] R. Rosenkranz, G. Frommeyer, Microstructures and properties of the refractory compounds TiSi<sub>2</sub> and ZrSi<sub>2</sub>, *Z. Met.kd.* 83 (9) (1992) 685–689.
- [44] C.J. Howard, R.J. Hill, B.E. Reichert, *Acta Crystallogr., Sect. B: Struct. Sci.* 44 (1988) 116.
- [45] A.G. Every, A.K. McCurdy, Table 3. Cubic system. Elements, in: Landolt–Börnstein–Group III Condensed Matter Numerical Data and Functional Relationships in Science and Technology, vol. 29a, Springer-Verlag, 1992.
- [46] D.D. Slagle, H.A. McKinstry, *J. Appl. Phys.* 38 (1967) 446–458.
- [47] P.E. Blöchl, Projector augmented-wave method, *Phys. Rev. B* 50 (1994) 17953–17979.
- [48] D. Vanderbilt, Soft self-consistent pseudopotentials in a generalized eigenvalue formalism, *Phys. Rev. B* 41 (1990) 7892–7895.
- [49] P.S. Spoor, J.D. Maynard, M.J. Pan, D.J. Green, J.R. Hellman, T. Tanaka, Elastic constants and crystal anisotropy of titanium diboride, *Appl. Phys. Lett.* 70 (1997) 1959–1961.
- [50] C.J. Smithells, E.A. Brandes, F.R. Institute, *Smithells Metals Reference Book*, Vol. 8, Butterworth-Heinemann, 1983.
- [51] Y. Le Page, P. Saxe, Symmetry-general least-squares extraction of elastic data for strained materials from *ab initio* calculations of stress, *Phys. Rev. B* 65 (2002) 104104.
- [52] H. Kimizuka, H. Kaburaki, Y. Kogure, Molecular-dynamics study of the high-temperature elasticity of quartz above the  $\alpha - \beta$  phase transition, *Phys. Rev. B* 67 (2003) 024105.
- [53] J. Purton, R. Jones, C.R.A. Catlow, M. Leslie, *Ab initio* potentials for the calculation of the dynamical and elastic properties of  $\alpha$ -quartz, *Phys. Chem. Miner.* 19 (1993) 392–400.
- [54] B. Holm, R. Ahuja, *Ab initio* calculation of elastic constants of SiO<sub>2</sub> stishovite and  $\alpha$ -quartz, *J. Chem. Phys.* 111 (1999) 2071.
- [55] R. Bechmann, Elastic and piezoelectric constants of alpha-quartz, *Phys. Rev.* 110 (1958) 1060–1061.
- [56] W.P. Mason, *Piezoelectric Crystals and their Applications to Ultrasonics*, Vol. 84, Van Nostrand, 1950, p. 508.
- [57] E. Gregoryanz, R.J. Hemley, H. Kwang Mao, P. Gillet, High-pressure elasticity of  $\alpha$ -quartz: instability and ferroelastic transition, *Phys. Rev. Lett.* 84 (2000) 3117–3120.
- [58] P.-F. Chen, L.-Y. Chiao, P.-H. Huang, Elasticity of magnesite and dolomite from a genetic algorithm for inverting Brillouin spectroscopy measurements, *Phys. Earth Planet. Inter.* 155 (1–2) (2006) 73–86.
- [59] P. Humbert, F. Plique, Propriétés élastiques de carbonates rhomboédriques monocristallines: calcite, magnésite, dolomie, *C. R. Acad. Sci. Paris* 275 (1972) 391–394.
- [60] H.R. Cutler, J.J. Gibson, K.A. McCarthy, *Solid State Commun.* 6 (1968) 431–433.
- [61] W.J. Alton, A.J. Barlow, *J. Appl. Phys.* 38 (1967) 3817–3820.
- [62] M. Nakamura, *Metall. Trans. A* 25A (1993) 331.
- [63] S.C. Chan, Y. Fang, M. Grimsditch, Z. Li, M. Nevitt, W. Robertson, E.S. Zoubolis, Temperature dependence of elastic moduli of monoclinic zirconia, *J. Am. Ceram. Soc.* 74 (1991) 1742–1744.
- [64] J. Nye, *Physical Properties of Crystals: Their Representation By Tensors and Matrices*, Oxford Science Publications, Clarendon Press, 1985.